PERGAMON

International Journal of Solids and Structures 38 (2001) 1707–1720

INTERNATIONAL JOURNAL OF SOLIDS and STRUCTURES

www.elsevier.com/locate/ijsolstr

An adaptive approach to limit analysis

Lavinia Borges [a,*], Nestor Zouain [a], Cyntia Costa [a], Raul Feijóo [b]

[a] *Department of Mechanical Engineering, Universidade Federal do Rio de Janeiro, P.O. Box 68503, 21945-970 Rio de Janeiro, RJ, Brazil*
[b] *Department of Computational Mechanics, Laboratório Nacional de Computação Científica, Rua Getúlio Vargas, 333, 25651-070 Petrópolis, RJ, Brazil*

Received 27 August 1999; in revised form 3 February 2000

Abstract

The main objective of this paper is to propose an adaptive mesh refinement procedure for finite element models in limit analysis. We use an 'a posteriori' indicator based on the local directional interpolation error and a recovering scheme to compute second derivatives of the finite element solution. The proposed mesh adaptation process gives improved results in localizing regions of rapid or abrupt variations of the variables, whose location is not known a priori. Limit analysis of bodies in plane strain and plane stress is considered in the applications. © 2001 Elsevier Science Ltd. All rights reserved.

Keywords: Limit analysis; Error estimation; Finite element; Adaptivity

1. Introduction

The main objective of this paper is to propose an adaptive mesh refinement procedure for limit analysis. This procedure uses an a posteriori estimator of the local directional interpolation error and a recovering scheme to compute the first and second derivatives of the finite element solution. The strategy presented here is an extension of the one presented by Borges et al. (1998, 1999) and Feijóo et al. (1997) wherein the estimator and the adaptive process were only defined for linear finite elements. Here we generalize the indicator and the adaptive procedure to include quadratic triangles.

The advantages of adapting meshes are well known. Furthermore, we place particular emphasis on the anisotropic mesh adaptation process, generated by the proposed directional indicator. The goal of that approach is to achieve a mesh-adaptive strategy accounting for mesh size refinement, as well as redefinition of the oriented element stretching. This way, along the adaptation process, the mesh turns aligned with the direction of maximum curvature of the function graph. This mesh adaptation procedure gives improved results in localizing regions of rapid or abrupt variations of the variables, whose location is not known a priori (Peiró, 1989; Peraire et al., 1990; Dompierre et al., 1995; Verfürth, 1996; Almeida et al., 1998;

* Corresponding author.
E-mail address: lavinia@serv.com.ufrj.br (L. Borges).

0020-7683/01/$ - see front matter
PII: S0020-7683(00)00131-1

Buscaglia and Dari, 1997). As a result, accurate representations of shocks, boundary layers, and other discontinuities are obtained.

Limit analysis deals with the direct computation of the load producing plastic collapse of a body – a phenomenon where, under constant stresses, kinematically admissible plastic strain rates take place. Localized plastic deformations or slip bands are present in many collapse situations. The accuracy in numerical solutions of limit analysis is seriously affected by local singularities arising from these localized plastic deformations. In limit analysis, an a priori error estimate, in a local sense as provided by the standard error analysis in the finite element method, is not available. Those facts disclose the need of a mesh refinement indicator which can be extracted a posteriori from the numerical solution.

Another feature of numerical limit analysis influenced by an oriented mesh adaptation procedure is the locking phenomenon.

The locking characteristics of finite elements are important in plane strain or axisymmetric limit analysis. Indeed, when Mises yield function is assumed, the exact velocity field satisfies the incompressibility condition. In these cases, the classical three-node finite element, that use linear interpolants for the velocity field, has a strong tendency to lock so that we use it only in plane stress problems. A curved triangular mixed element was specially created to face the locking problem (Borges et al., 1996) in the framework of limit analysis. For this element, an efficient adaptive strategy demands an error distribution assumption richer than piecewise constant by element.

In this paper, firstly, the theoretical framework of limit analysis is presented. Following this, some issues of the adopted techniques for estimating the interpolation error, based on derivative recovery schemes, are discussed. Finally, we propose a directional interpolation error estimator and adaptive mesh refinements for limit analysis applications.

2. Limit analysis

Under the assumption of proportional loading, the limit analysis problem consists in finding a load factor α such that the body undergoes a plastic collapse when subject to the reference loads F uniformly amplified by α. In turn, a system of loads produces plastic collapse if there exists a stress field in equilibrium with these loads which is plastically admissible, and related, by the constitutive equations, to a plastic strain rate field being kinematically admissible (Lubliner, 1990).

Thus, the limit analysis problem consists in finding $\alpha \in \mathbb{R}$, a stress field $T \in W'$, a plastic strain rate field $D^{\mathrm{p}} \in W$ and a velocity field $v \in V$ such that

$$D^{\mathrm{p}} = \mathscr{D}v, \quad v \in V, \tag{1}$$

$$T \in S(\alpha F), \tag{2}$$

$$T \in \partial X(D^{\mathrm{p}}). \tag{3}$$

The meaning of these relations and the notation are explained in the following. Eq. (1) imposes that the collapse plastic strain rate D^{p} is related to a kinematically admissible velocity field v by means of the tangent deformation operator $\mathscr{D}$ (V and W are the space of admissible velocities and strain rate fields, while V' and W' are the spaces for loads and stress fields). The symbol $S(\alpha F)$ in Eq. (2) denotes the set of all stress fields in equilibrium with the given system of forces αF, that is satisfying the principle of virtual power:

$$\int_{\mathscr{B}} T \cdot \mathscr{D}v \, \mathrm{d}\mathscr{B} = \alpha \left(\int_{\mathscr{B}} bv \, \mathrm{d}\mathscr{B} + \int_{\Gamma_\tau} \tau v \, \mathrm{d}\Gamma \right) \quad \forall v \in V, \tag{4}$$

where b and τ are body and surface loads, respectively, and Γ_τ, the region of Γ where tractions are prescribed.

In Eq. (3), the constitutive relation describing an elastic ideally plastic material is given. The symbol $\partial X(D^{\mathrm{p}})$ denotes the subdifferential of the plastic dissipation function X, which is the set of all stress fields, such that

$$X(D^{\mathrm{p}*}) - X(D^{\mathrm{p}}) \geqslant \int_{\mathscr{B}} T \cdot (D^{\mathrm{p}*} - D^{\mathrm{p}})\, \mathrm{d}\mathscr{B} \quad \forall D^{\mathrm{p}*} \in W. \tag{5}$$

The dissipation function is related to the set P of plastic admissible stress fields by

$$X(D^{\mathrm{p}}) = \sup_{T^* \in P} \int_{\mathscr{B}} T \cdot \mathscr{D}v\, \mathrm{d}\mathscr{B}. \tag{6}$$

Frequently, the set P is defined as

$$P = \{T \in W' \,|\, f(T) \leqslant 0 \text{ in } \mathscr{B}\}, \tag{7}$$

where the above inequality is then understood as imposing that each component f_k, which is a regular convex function of T, is non-positive. Then, at any point of $\mathscr{B}$, Eq. (3) is equivalent to the normality rule $D^{\mathrm{p}} = \nabla f(T)\,\dot{\lambda}$, where $\nabla f(T)$ denotes the gradient of f, and $\dot{\lambda}$ is the $\widehat{m}$-vector field of plastic multipliers. At any point of $\mathscr{B}$, the components of $\dot{\lambda}$ are related to each plastic mode in f by the complementarity condition $\dot{\lambda} \geqslant 0$, $f \leqslant 0$ and $f\dot{\lambda} = 0$ (these inequalities hold componentwise).

The classical extremum principles of limit analysis, that is the kinematical, statical and mixed formulations, can be derived from the optimality conditions (1)–(3) (Christiansen, 1996; Borges et al., 1996). The discretized versions of these formulations lead to a single type of finite dimensional problem, which can be cast in four strictly equivalent forms, namely the statical, mixed and kinematical discrete formulations, and the set of discrete optimality conditions.

2.1. Discrete model

The discrete limit analysis problem consists in finding a load factor $\alpha \in \mathbb{R}$, a stress vector $T \in \mathbb{R}^q$, a velocity vector $v \in \mathbb{R}^n$ and a plastic multipliers vector $\dot{\lambda} \in \mathbb{R}^m$ such that the system represented by a deformation matrix $B : \mathbb{R}^n \to \mathbb{R}^q$ and a convex function $f(T) \in \mathbb{R}^m$ undergoes plastic collapse for some load being proportional to a given force vector $F \in \mathbb{R}^n$. It is assumed that all rigid motions are ruled out by the kinematical constraints so that the kernel of matrix B contains only the null velocity vector.

The discretized version of the limit analysis formulation leads to a finite dimensional problem that can be seen as a discrete version of Eqs. (1)–(3), that is

$$Bv - \nabla f(T)\,\dot{\lambda} = 0, \tag{8}$$

$$B^{\mathrm{T}} T - \alpha F = 0, \tag{9}$$

$$Fv = 1, \tag{10}$$

$$f_j(T)\dot{\lambda}_j = 0, \quad f_j(T) \leqslant 0, \quad \dot{\lambda}_j \geqslant 0, \quad j = 1, \ldots, m. \tag{11}$$

A Newton-like algorithm for solving this discrete problem is described by Borges et al. (1996) and is not discussed in the present work.

Many issues arise concerning the choice of a finite element interpolation, such as convergence and (global) error estimate. In the following, we comment briefly on the choice of the elements and also the estimator for the interpolation error used here as a mesh refinement indicator.

For plane strain, and in solids with symmetry of revolution, we use a curved triangular mixed elements having (i) six nodes intended for the C^o quadratic interpolation of geometry and velocities, (ii) three nodes, at vertices, for the discontinuous linear interpolation of the deviatoric stresses, and (iii) piecewise constant interpolation for the mean stress (Borges et al., 1996). This mixed element is specially created to face the locking problem.

Localized plastic deformations or slip bands are present in most collapse situations. Accuracy in the numerical solution of limit analysis is seriously affected by local singularities arising from these localized plastic deformations. One possible approach in order to overcome this difficulty is to add more grid-points where the solution presents those singularities. Accordingly, it becomes necessary not only to identify these regions but also to obtain a good equilibrium between the refined and unrefined regions, for an optimal overall accuracy (Verfürth, 1996).

The choice of a variable to be used to control the adaptive process is not obvious. To capture the discontinuities, the natural choice is one of the components of the velocity vector field provided we can estimate in advance which component is suitable to this aim. However, this is not an easy task for a general problem. Unlike the velocity field, the scalar field of plastic multipliers may be used as a control variable without the previous disadvantage. These plastic factors are proportional to the modulus of the plastic strain rates, as indicated by Eq. (8). Hence, the plastic multipliers clearly indicate the region where localized plastic deformations or slip bands are present. As a consequence, the local singularities arising from these localized plastic deformations are also detected in this way. Based on this argument, the scalar field of plastic multipliers appears to be a good choice as a control variable and it is adopted for most of the applications.

Finally, it is worth discussing whether, for quadratic triangles, the second derivatives are able to assure reliable estimates for the interpolation error of the computed solution or we need to imagine an indicator based on higher derivatives of the interpolated field. While aiming to answer this question we note the following:

(1) According to Dompierre et al. (1995), even when using interpolation functions of degrees higher than one, the informations provided by second derivatives are sufficient to estimate the interpolation error.

(2) In the mixed element used here, the interpolations are C^o quadratic for velocities and geometry, piecewise constant for mean stress, and piecewise linear for deviatoric stress. This determines, in the discrete version of limit analysis, Eqs. (8)–(11), three plastic admissibility constraints at the vertices, ensuring plastic admissibility throughout the element. Accordingly, the associated plastic flow equations involve three plastic multipliers for each element, defined at the vertices of the triangle (Borges et al., 1996). This suggests a linear approximation for the smoothed scalar field of plastic multipliers.

The above arguments justify the application of a directional indicator for the interpolation error, based on second derivatives, using the modulus of the strain rate field as control variable in the adaptive mesh refinement strategy for limit analysis.

3. Estimator for the interpolation error

In the methods considered here, gradients and/or Hessians of the solutions, obtained on a given mesh, are smoothed and then used in the interpolation error estimator. It is well known that in elliptic problems, the derivatives of the approximate solution, $u_h \in V_h$ (V_h is the interpolation space) are superconvergent in some interior points of the elements. That is, in these points the derivatives of the finite element solution exhibit higher accuracy than the one normally expected. Although no analogous result exists for limit analysis, the proposed indicator is motivated by superconvergence. That is, it is focused on recovering the

Hessian with a higher order of accuracy than that naturally obtained from the finite element approximation. Therefore, in the proposed procedure, it is necessary to recover the Hessian matrix from the information given by the finite element solution u_h. Almost all algorithms aimed to recover the Hessian matrix use first derivative information. Recovering first and second derivatives are the main issues of the following section.

3.1. The interpolation error as an indicator of the approximate solution

We present an anisotropic a posteriori error estimator for the difference between a given function u and a discrete function $U \in V_h$ which is a good approximation of u in Ω in the sense that

$$\|u - U\|_{L^p(\Omega)} \leqslant C\|u - \Pi u\|_{L^p(\Omega)} \tag{12}$$

with $\Pi : W^{2,p}(\Omega) \to V_h$ denoting an operator whose approximation properties are similar to the Clement interpolation operator (Clément, 1975). That is (Almeida et al., 1998), there exists a constant C such that

$$\|u - u_h\|_{L^p(\Omega)} \simeq C\|\mathscr{H}_R(u_h(x))(x - x_0)(x - x_0)\|_{L^p(\Omega)}, \tag{13}$$

where $\mathscr{H}_R(u_h(x))$ denotes the recovered Hessian matrix obtained from the information given by the finite element solution u_h. This shows that the interpolation error at some point x, where $\|x - x_0\|$ is small enough, is governed by the behavior of the second order derivative. Thus, the interpolation error is not distributed in an isotropic way around the point x_0, i.e., the error depends on the direction $x - x_0$ and the recovered Hessian matrix value in this point, $\mathscr{H}_R(u(x))$.

The above result suggests the use of Eq. (13) as a *directional* error estimator in the terminology used by Peiró (1989) and Peraire et al. (1990). Since the recovered Hessian matrix is not positive definite, it cannot be taken as a metric tensor. As an alternative, Peiró introduced the metric tensor:

$$\mathbf{G} = \mathbf{Q}\mathbf{\Lambda}\mathbf{Q}^{\mathrm{T}}, \tag{14}$$

where $\mathbf{Q}$ is the matrix of eigenvectors of the recovered Hessian matrix, the matrix $\mathbf{\Lambda} = \mathrm{diag}\{|\lambda_1|, |\lambda_2|\}$, and $\{|\lambda_i|, i = 1, 2\}$, are the absolute value of the associated eigenvalues ($|\lambda_1| \leqslant |\lambda_2|$). According to this definition, the metric tensor field $\mathbf{G}$ is at least positive semi-definite. In particular, a zero eigenvalue poses no difficulty since it leads to infinite mesh sizes that are inhibited by the element size limitation or by the bounds of the computational domain.

Following the above ideas, Dompierre et al. (1995), introduced an error estimator associated with the size of element edges and Buscaglia and Dari (1997) used Eq. (14) in a quality mesh indicator. The interpolation error estimator introduced herein is a variation of the first one. Instead of considering an error estimator associated to the element edge length, it is proposed to use another one that provides a measure of the second derivative contribution in each element (Venére, 1996). Considering a given finite element mesh $\mathfrak{I}$ of the domain Ω, the indicator value corresponding to each element $T \in \mathfrak{I}$ is defined by the following expression (Feijóo et al., 1997; Verfürth, 1996; Ainsworth and Oden, 1997; Zienkiewicz and Zhu, 1987):

$$\eta_T = \left\{ \int_T [\mathbf{G}(u_h(x_0))(x - x_0)(x - x_0)]^p \mathrm{d}\Omega \right\}^{1/p}, \tag{15}$$

where x_0 is the center of this element.

The global indicator η is given by

$$\eta = \left(\sum_{T \in \mathfrak{I}} \eta_T^p \right)^{1/p}. \tag{16}$$

3.2. Derivatives recovery

Several approaches have been proposed, in the framework of the Finite Element Method, in order to recover first derivatives. This subject may be found, for instance, in Zienkiewicz and Zhu (1992a,b). The *weighted average* is one among these procedures, and it is briefly summarized in the sequel.

The recovery approach quoted weight average consists of turning the inter-elements discontinuous field ∇u_h into a continuous field $\nabla_R u_h$. This is made by employing the same element basis functions used to construct the approximation u_h to compute the field ∇u_h. Then, a weighted average of ∇u_h, computed on the elements surrounding a node N is adopted as the value $\nabla_R u_h(\mathbf{X}_N)$ of the recovered gradient at this node ($\mathbf{X}_N$ is the coordinate of node N). The weighted average is computed using weights given by the inverse of the distance between the node N and the points of superconvergence of the gradient (the center of the element in the case of linear triangles and the Gauss points near midside nodes in the case of quadratic triangles (Zienkiewicz and Zhu, 1992a,b). The weights can also be defined by the area of the elements surrounding the node.

Second derivatives can also be recovered by using the same approaches used for the first derivative recuperation. In fact, taking $\nabla_R u_h$ as a new field, we can reapply the algorithm in order to find $\nabla_R(\nabla_R u_h)$. The symmetric part of the approximation is retained in order to ensure the symmetry of the recovered Hessian matrix.

In order to approximate functions presenting strong variations in the derivatives, the adapted mesh turns to be oriented by means of the stretching of its elements in the direction of maximum curvature of the function graph. Whenever this stretching is very large, it may cause poor precision when computing weighted averages. To overcome this situation, the original domain Ω_T is locally transformed into a standard unstretched domain Ω_T^*. For instance, when using mesh generators based on the *advancing front technique* (Peiró, 1989; Peraire et al., 1990; Fancello et al., 1990, 1991; de Oliveira et al., 1997; Dari and Vénere, 1994; Venére, 1996) this domain transformation is naturally chosen in accordance with the domain mapping which is a part of the mesh generation algorithm. This is the procedure adopted in the present work and is described in the following:

Considering the neighborhood of an arbitrary node, N (Fig. 1), the mesh generation algorithm tends to create triangular elements which are equilateral when viewed in the transformed domain given by the following operator:

$$\mathbf{S}(N) = \frac{1}{s(N) * h(N)}\mathbf{e}_1 \otimes \mathbf{e}_1 + \frac{1}{h(N)}\mathbf{e}_2 \otimes \mathbf{e}_2, \tag{17}$$

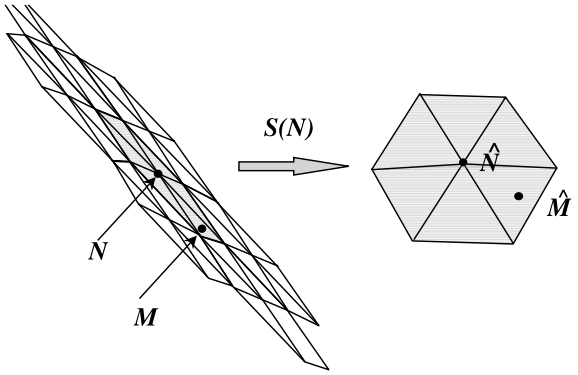

Fig. 1. Transformed domain defined by the advancing front technique.

where $\mathbf{e}_i(N), i = 1, 2$ are the eigenvectors of the Hessian matrix $\mathscr{H}_R(u_h(N))$, the length $h(N)$ is the element size in the $\mathbf{e}_2$ direction, and $s \geqslant 1$ is the element stretching in the $\mathbf{e}_1$ direction of the generated mesh at node N. Those parameters are all dynamically defined along the mesh adaptation process. The selection of these parameters is discussed in the next section.

Finally, the mapping which transforms the stretched element into the standard (equilateral) triangle is written as

$$\mathbf{x}_M = \mathbf{S}(N)(\mathbf{X}_M - \mathbf{X}_N). \tag{18}$$

The notation above is as follows: M is a generic point belonging to some element adjacent to the node N; the coordinates $\mathbf{X}_N$, $\mathbf{X}_M$ and $\mathbf{x}_M$ denote the point N and M before and after the mapping, respectively.

4. Adaptive procedure

The present adaptive procedure takes into account the global error indicator, η, given by Eq. (16), for each triangulation $\mathfrak{I}_k$. Then, the objective is to find a new mesh $\mathfrak{I}_{k+1}$, with a given number of elements Nel. This new finite element mesh is generated trying to produce a uniform distribution of the interpolation error estimator over all elements.

Our remeshing algorithm is based on the advancing front technique (Fancello et al., 1990, 1991; Oliveira et al., 1997; Dari and Vénere, 1994; Vénere, 1996). In this technique, the mesh generator tries to build equilateral triangles in the metric defined by the variable metric tensor $\mathbf{S}$ defined by Eq. (17). To evaluate the mapping parameters, we proceed as follows:

(1) Compute η_T in each element and then the global quantity η.

(2) Given a number of elements Nel in the new adapted mesh, the expected local indicator is given by

$$\eta^* = \frac{\eta}{\sqrt{\text{Nel}}}. \tag{19}$$

(3) The decreasing or increasing rate of the element size is estimated by

$$\beta_T = \left(\frac{\eta^*}{\eta_T}\right)^{1/3}. \tag{20}$$

From this rate distribution β_T, computed elementwise, nodal values are then obtained. Different approaches can be selected to this end. For instance, this operation may be based on the same scheme used to compute derivatives. The resulting nodal rate value is denoted by $\beta(N)$.

(4) The size of the new element, to be generated at node N, is

$$h_{k+1}(N) = \beta(N) h_k(N). \tag{21}$$

If necessary, the threshold values for the new element size are then enforced as

$$\underline{\alpha} * h_k \leqslant h_{k+1} \leqslant \overline{\alpha} * h_k \leqslant L, \tag{22}$$

where L represents the characteristic length of the domain Ω. The two parameters above, $\underline{\alpha}$ and $\overline{\alpha}$, are used in order to ensure progressive mesh adaptation.

(5) The stretching factor s at node N is defined by

$$s(N_k) = \sqrt{\frac{|\lambda_2|}{|\lambda_1|}}, \tag{23}$$

where $|\lambda_1| \leqslant |\lambda_2|$ are the absolute eigenvalue of the Hessian matrix $\mathscr{H}_R(u_h(N))$. This stretching factor must be bounded in order to ensure that the new length of the element in the direction $\mathbf{e}_1, sh_{k+1}$, is not greater than the characteristic length L of the domain Ω, i.e., $s \leqslant L/h_{k+1}$.

(6) The new size distribution, h_{k+1} is then uniformly scaled. Due to the limitation on the values of h and s, the number of elements in the new adapted mesh may be different from the expected Nel. To enforce the required new number of elements, the elements size h is modified as follows:

$$h_{k+1} \leftarrow \sqrt{\frac{\mathrm{Nel}_{\mathrm{new}}}{\mathrm{Nel}}} h_{k+1} \quad \text{with } \mathrm{Nel}_{\mathrm{new}} = \frac{4}{\sqrt{3}} \int_{\Omega} \frac{2}{sh^2} \mathrm{d}\Omega. \tag{24}$$

The adaptive strategy described above is repeated until the interpolation error estimator in the mesh, $\mathfrak{I}_k$, becomes lower than a given admissible relative error $\overline{\gamma}$, that is until

$$\frac{\eta_k}{(\|u_h\|_{L_2(\Omega)} + \eta_k)^{1/2}} \leqslant \overline{\gamma}. \tag{25}$$

4.1. Summary of the adaptive mesh algorithm

We summarize below the proposed algorithm for an adaptive mesh refinement strategy for limit analysis problems:

Adaptive procedure for limit analysis

Repeat

1. **Limit analysis**
   - Apply the Newton-like algorithm for solving the discrete limit analysis. Choose a scalar field to be used to control the adaptive process.
2. **First derivative recovery** (Section 3.2)

   For each node in the triangulation $\mathfrak{I}_k$
   - Define the *patch* associated to node N.
   - Compute the metric tensor $\mathbf{S}(N)$, from information about the mesh shape around the node N, defined by the known parameters $s(N)$, $h(N)$, $\mathbf{e_1}$ and $\mathbf{e_2}$.
   - Transform all the elements of the *patch*.
   - Compute the gradients $\mathrm{grad}\, u_h$ in each transformed element.
   - Using the recovering algorithm, compute $\mathrm{grad}_R u_h(N)$.
   - Transform the gradient $\mathrm{grad}_R u_h(N)$ to the original domain, by means of: $\nabla_R u_h(N) = \mathbf{S}^{\mathrm{T}}(N)\ \mathrm{grad}_R u_h(N)$.
3. **Second derivative recovery**
   - Compute $\nabla_R(\nabla_R u_h(N))$, by repeating step 2, for each component of $\nabla_R u_h(N)$.
   - Retain the symmetric part of $\nabla_R(\nabla_R u_h(N))$ to define $\mathscr{H}_R(u_h(N))$.
4. **Interpolation error estimation** (Section 3.1.)

   For each element in the the triangulation $\mathfrak{I}_k$
   - Compute the metric tensor $\mathbf{G}$.
   - Compute the local indicator η_T.

   Compute the global indicator η

   For a given Nel, estimate η^*
5. **Adaptive procedure**

   For each node in the the triangulation $\mathfrak{I}_k$
   - Compute h_{k+1}, s_{k+1}, $(\mathbf{e_1})_{k+1}$ and $(\mathbf{e_2})_{k+1}$.
   - Scale h_{k+1}.

6. **Generate a new mesh** $\Im_{k+1}$.
Until $\frac{\eta_k}{\left(\|u_h\|_{L_2(\Omega)}+\eta_k\right)^{1/2}} \leqslant \overline{\gamma}$

5. Numerical applications

The first two examples of application are plane stress problems where linear triangles are used. A third example, under plane strain condition, is then presented as another application of the adaptive limit analysis procedure combined with the mixed element mentioned before. In these applications, the materials obey the Mises yield criterion, with the yield stress denoted by σ_Y.

5.1. Square slab with symmetrical internal slit

Limit analysis of a square slab with a symmetrical internal slit subjected to traction is considered here. The theoretical collapse mechanism of this slab presents localized deformation in the form of slip bands emanating from the roots of the crack. This is also obtained in the numerical solution, as shown in Fig. 2.

We analyze the behavior of the adaptive strategy, when choosing the x-component of the velocity field or, alternatively, the plastic multiplier field, as the control variable. As shown in Fig. 3, both are effective as a basis for the directional error estimator. The isovalues for the plastic deformation and for the local

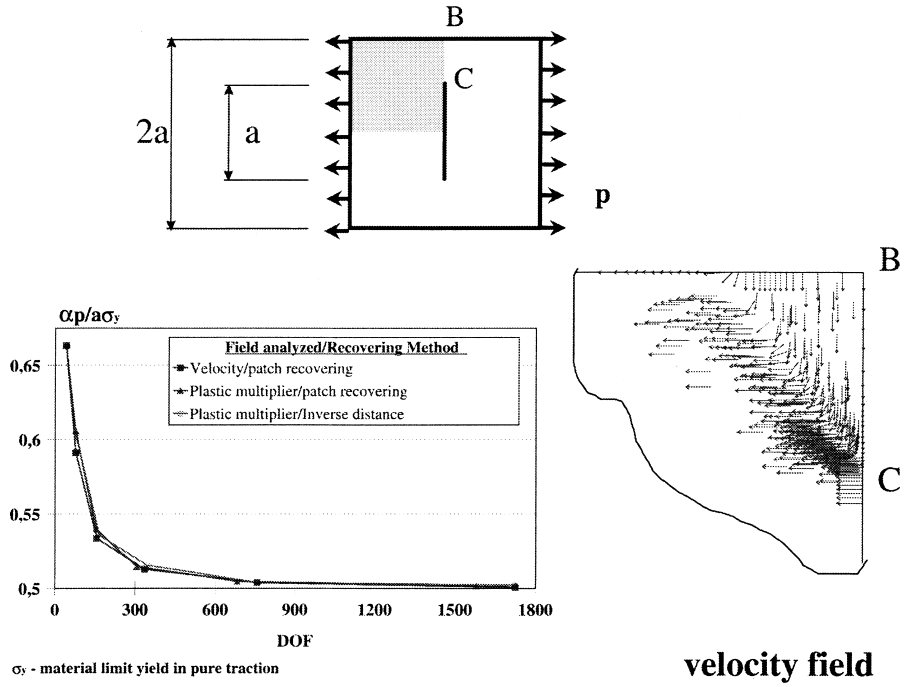

Fig. 2. Slab with an internal slit – collapse load evolution and velocity field.

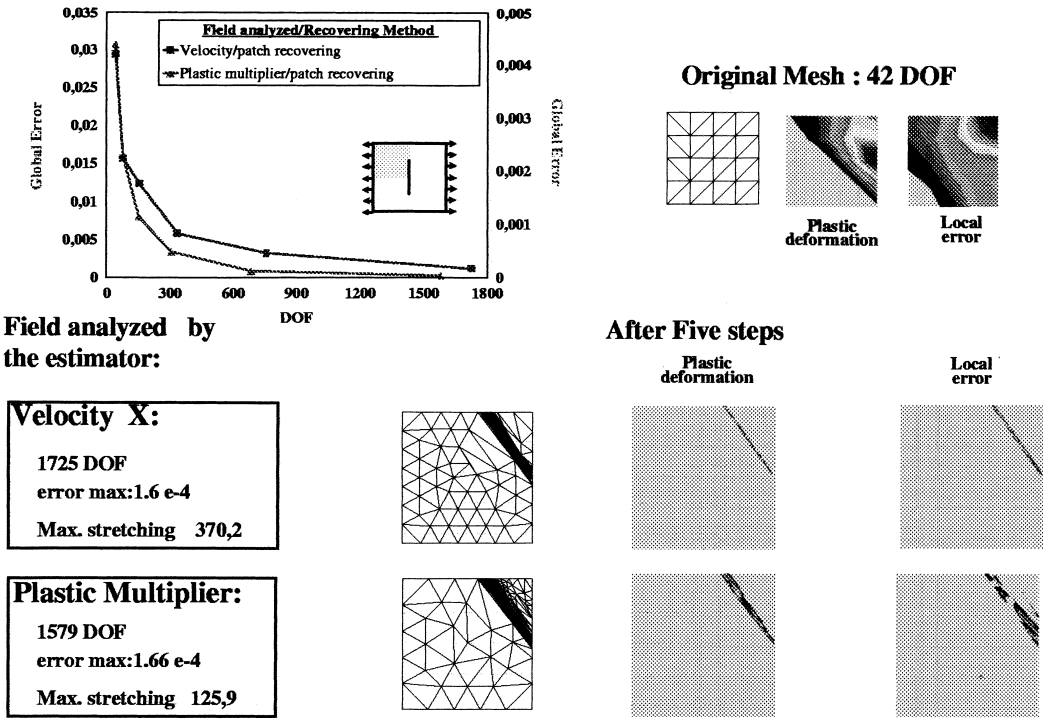

Fig. 3. Slab with an internal slit – error, mesh and plastic deformation.

interpolation error show that the proposed procedure is also effective in capturing the localized plastic deformation. Indeed, it increases the nodal points of the mesh only in the neighborhood of the region where the discontinuities take place. Moreover, it constructs elements which are aligned and stretched in the direction of slip bands.

We obtain 27% reduction in the collapse load approximation (Fig. 2) by means of five adaptation steps. It is worth noting that the kinematical principle adopted in this case yields an upper bound to the exact collapse load and so, this reduction during the adaptive process is expected.

5.2. A thin square slab, with a central circular hole and subject to traction

This is a plane stress problem that was analyzed considering three values of the ratio between the diameter d of the hole and the length L of the slab side. The numerical results for the collapse factor are plotted in Fig. 4 and compared to analytical lower and upper bounds (Gaydon and Mc Crum, 1954).

For $d/L = 0.2$, the velocity field presents a slip band which runs from the unstressed edge of the slab and meets the hole in the transversal axis of symmetry. The behavior of this numerical velocity field complies with that foreseen in the analytical solution that identifies slip bands for ratios d/L lower than 0.4. The analytical collapse mechanism for $d/L > 0.6$ imposes that each quarter of the slab rotates as a rigid body producing plastic hinges at its narrowest parts, that is, along the axes of symmetry. All of those kind of mechanisms are detected in the numerical solution, as can be observed in Fig. 4, where plastic region is the darkest one.

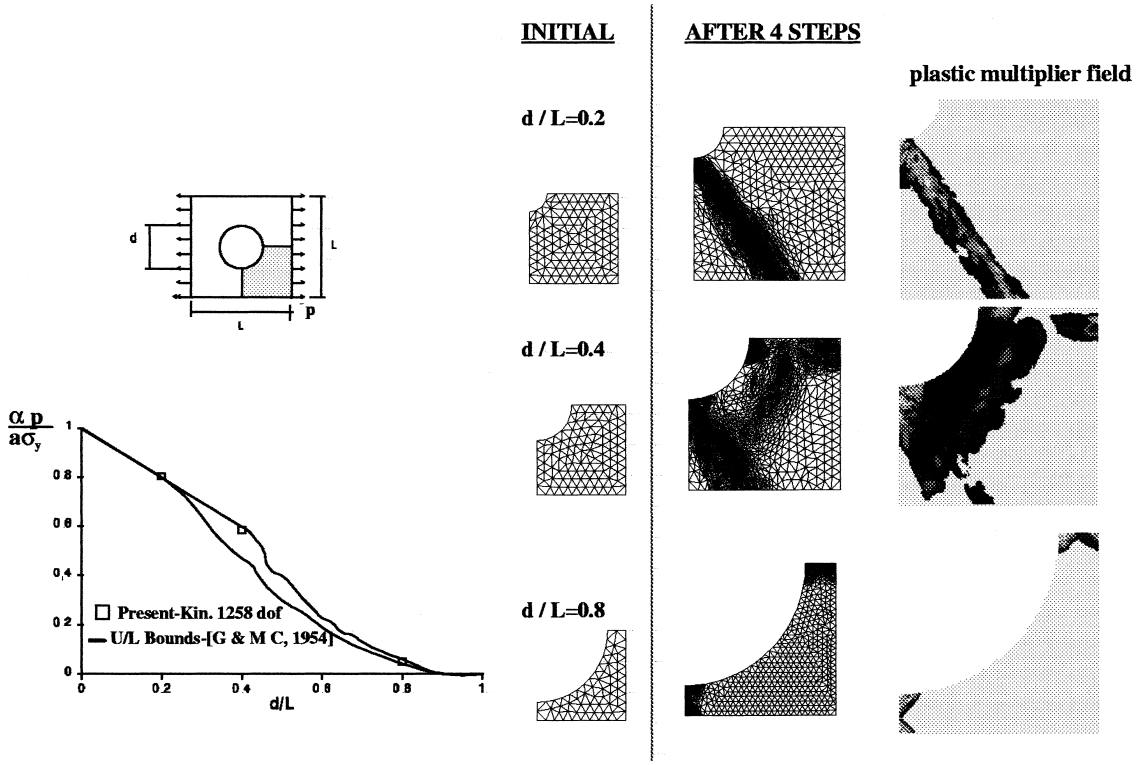

Fig. 4. Slab with circular cutout – collapse load, final meshes and plastic region.

5.3. Frictionless extrusion through a square die

In the limit analysis model for extrusion processes, we consider a state of steady plastic flow. In this process, a large amount of plastic deformation has already taken place, and the stress and velocity fields are taken as constant in time in an Eulerian sense (Lubliner, 1990). Assuming the Mises yield criterion and plane strain, the slip-line theory applies. This analytical approach gives, in general, an upper bound for the piston pressure that produces unbounded plastic flow. However, for the present situation, of both problems, the slip-line solution provides not only an upper bound for the extrusion pressure but the exact pressure (Lubliner, 1990).

We have simulated two plane strain frictionless extrusion processes. In the first case we consider a reduction of $2/3$ and in the second one the reduction is $1/5$. Because of the symmetry, we modeled only the upper half, as shown in Figs. 5 and 6.

Figs. 5 and 6 illustrate the numerical solutions obtained after the adaptation steps. In the two cases, the adaptive strategy made it possible to capture the slip bands and to identify the regions that present distributed plastic deformation. These regions are defined by the colorful part in the figure representing the isovalues for plastic multiplier field. Notice that the numerical solution is very close to the analytical slip-line field due to Hill (Lubliner, 1990), sketched besides the numerical solution.

For the $2/3$-reduction problem, and at the end of the adaptation process, we attain an extrusion pressure of $1.9690\sigma_Y$. The exact value, obtained by the slip-line theory, is $1.9790\sigma_Y$. In the same way, for a reduction of $1/5$ the numerical solution obtained is $1.4781\sigma_Y$ and the analytical one is $1.4842\sigma_Y$. Therefore, in the two cases, the difference between the numerical extrusion pressure and the analytical one is no greater than 0.5%.

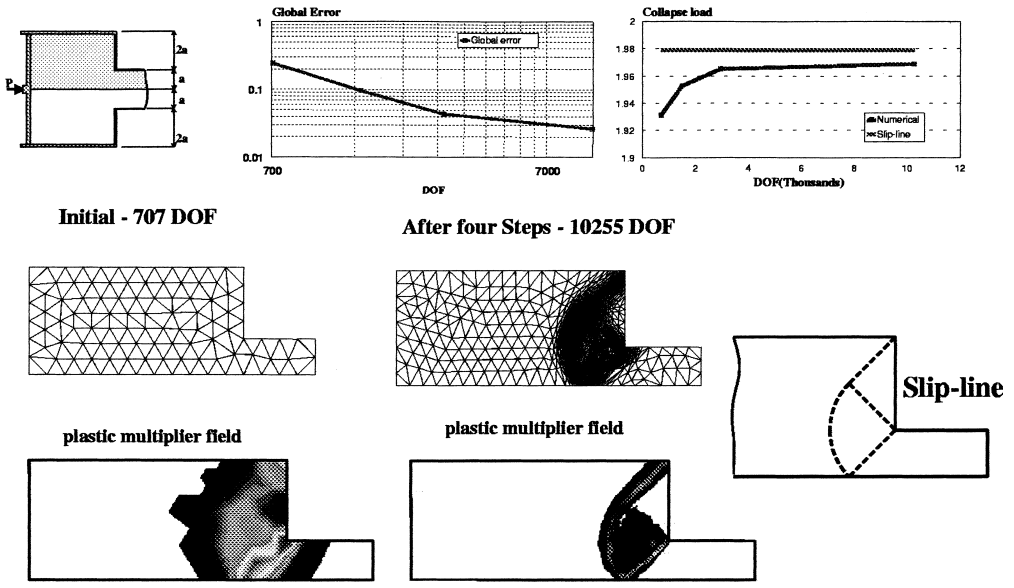

Fig. 5. Frictionless extrusion through a square die – reduction 2/3.

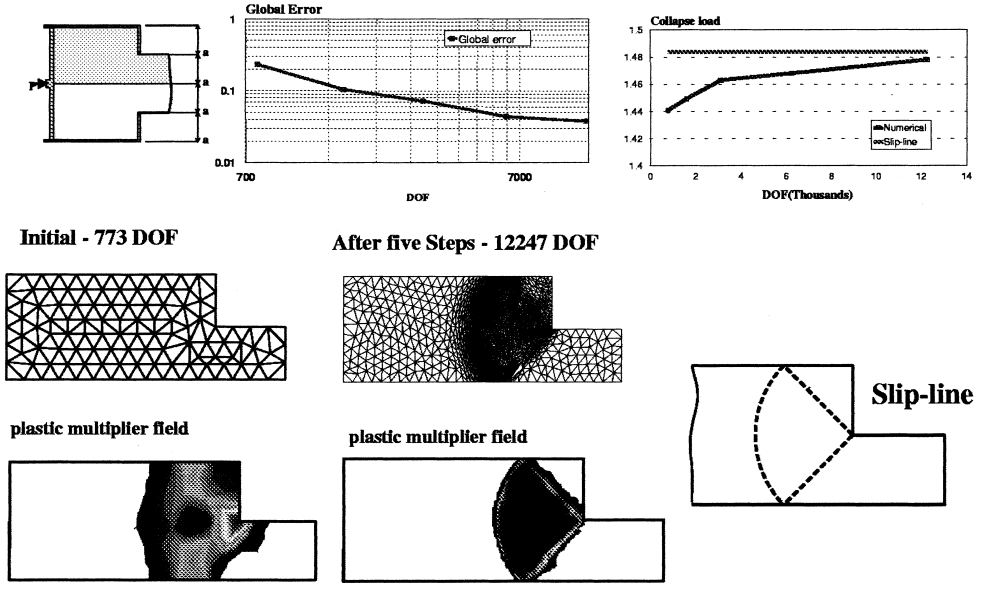

Fig. 6. Frictionless extrusion through a square die – reduction 1/2.

6. Conclusions

An anisotropic adaptive procedure, based on an a posteriori estimate of the local directional interpolation error, and using recovery techniques for the Hessian matrix has been presented in this paper. The proposed method is able to capture discontinuities arising from localized plastic deformations during

plastic collapse. As a consequence, the mesh adaptation significantly improves the numerical evaluation of the collapse load.

The numerical applications confirm the feasibility of the approach, that is, the computation of the mesh refinement indicator is less expensive than the calculation of the numerical solution. In all the analyzed applications, the computational time for error evaluation is about 1% of the whole time spent in the limit analysis algorithm.

Other recovery techniques can be also adopted instead of the weighted average proposed herein. One of them is the *path recovery technique* introduced by Zienkiewicz and Zhu (1992a,b). This approach, associated to an interpolation error estimator based on second derivative recovery, for linear finite elements, was presented by Borges et al. (1998, 1999) in the context of limit analysis, and by Almeida et al. (1998) for computational fluid dynamics.

In this work, the new adapted finite element mesh is generated trying to produce a uniform distribution of the local indicator over all elements. Almeida et al. (1998) proposed an adaptive analysis in which the mesh is adapted with the aim to distribute the indicator local values with minimum computational cost (*optimal adaptive analysis*). In this procedure, for a given number of desired elements, a new mesh is generated such that the distribution $h_{\text{new}}(N)$ for all nodes, minimizes the global indicator value. This procedure can also be incorporated into the limit analysis procedure.

References

Ainsworth, M., Oden, J.T., 1997. A posteriori error estimation in finite element analysis. Computer Methods in Applied Mechanics Engineering 42, 1–88.

Almeida, R.C., Feijóo, R.A., Galeão, A.C.N., Padra, C., Simões, R., 1998. Adaptive finite element computational fluid dynamics using an anisotropic error estimator. Computational Mechanics – New Trends and Applications. Fourth World Congress on Computational Mechanics, Argentina.

Borges, L., Feijóo, R.A., Padra, C., Zouain, N., 1998. A directional error estimator for adaptive finite element analysis. Computational Mechanics – New Trends and Applications. Fourth World Congress on Computational Mechanics, Argentina.

Borges, L.A., Zouain, N., Huespe, A.E., 1996. A nonlinear optimization procedure for limit analysis. European Journal of Mechanics A/Solids 15, 487–512.

Borges, L.A., Feijóo, R.A., Zouain, N., 1999. A directional error estimator for adaptive limit analysis. Mechanics Research Communications 26 (5), 555–563.

Buscaglia, G.C., Dari, A., 1997. Anisotropic mesh optimization and its application in adaptivity. International Journal for Numerical Methods in Engineering 40, 4119–4136.

Christiansen, E., 1996. Limit analysis of collapse states. In: P.G. Ciarlet and J.L. Lioan (Eds.), Handbook of Numerical Analysis, vol. 4. North-Holland, Amsterdam, pp. 193–312.

Clément, P., 1975. Approximation by finite element functions using local regularization. RAIRO Anal. Numer. R-2, 77–84.

Dari, E., Vénere, M.J., 1994. Finite element 3-D mesh generation using the advancing front technique. MECOM'94, Mar del Plata, Argentina.

Dompierre, J., Vallet, M.G., Fortin, M., Habashi, W.G., Aït-Ali-Yahia, D., Boivin, S., Bourgault, Y., Tam, A., 1995. Edge-based mesh adaptation for cfd. Conference on Numerical Methods for the Euler and Navier-Stokes Equations, Montreal pp. 265–299.

Fancello, E., Guimarães, A.C.S., Feijóo, R.A., 1990. Aranha – gerador de malhas 2d para elementos finitos triangulares de 3 e 6 nós. XI Ibero Latin American Congress in Computational Methods In Engineering I, 983–996 (in Portugese).

Fancello, E., Guimarães, A.C.S., Feijóo, R.A., Vénere, M.J., 1991. Geração de malhas 2-d em programação orientada a objetos. XI Brazilian Congress of Mechanical Engineering 635–638 (in Portuguese).

Feijóo, R.A., Borges, L., Zouain, N., 1997. Estimadores a posteriori y sus aplicaciones en el análisis adaptativo. Technical Report 01/97, COPPE/UFRJ.

Gaydon, F.A., Mc Crum, A.W., 1954. A theoretical investigation of the yield point loading of a square plate with a central circular hole. Journal of the Mechanics and Physics 2, 156–169.

Lubliner, J., 1990. Plasticity Theory. Macmillan, New York.

de Oliveira, M., Guimarães, A.C.S., Feijóo, R.A., Vénere, M.J., Dari, E., 1997. An object oriented tool for automatic surface mesh generation using the advancing front technique. International Journal for Latin America Applied Research 27, 39–49.

Peiró, J., 1989. A finite element procedure for the solution of the Euler equations on the unstructured meshes. Ph.D. Thesis, Department of Civil Engineering, University of Swansea, UK.

Peraire, J., Morgan, K., Peiró, J., 1990. Unstructured finite element mesh generation and adaptive procedures for CFD. AGARD Publication No. 464: Applications of Mesh Generation to Complex 3-D Configurations 18.1–18.12.

Venére, M.J., 1996. Técnicas Adaptativas para el Método de Elementos Finitos en Dos y Tres Dimensiones. Ph.D. Thesis, Instituto Balseiro, Centro Atómico Bariloche, Argentina.

Verfürth, R., 1996. A Posteriori Error Estimation and Adaptive Mesh Refinement Techniques. Series: Advances in Numerical Mathematics, Wiley-Teubner.

Zienkiewicz, O.C., Zhu, J.Z., 1987. A simple error estimator and adaptive procedure for practical engineering analysis. International Journal for Numerical Methods in Engineering 24, 333–357.

Zienkiewicz, O.C., Zhu, J.Z., 1992a. The superconvergent patch recovery and a posteriori error estimator. part 1: The recovery technique. International Journal for Numerical Methods in Engineering 33, 1331–1364.

Zienkiewicz, O.C., Zhu, J.Z., 1992b. The superconvergent patch recovery and a posteriori error estimator. part 2: Error estimates and adaptivity. International Journal for Numerical Methods in Engineering 33, 1365–1382.